SCEC 2020 Final Report – SCEC ID 20203

Trenching the Causative faults of the 2019 Ridgecrest sequence

Ian Pierce[1,2]
Rich Koehler[2]
Alana Williams[3]
Ramon Arrowsmith[3]

[1]Centre for Observation and Modeling of Earthquakes, Tectonics, and Volcanoes, University of Oxford, UK
[2]Nevada Bureau of Mines and Geology, University of Nevada, Reno
[3]Arizona State University, Tempe, Az

Abstract

The 2019 Ridgecrest earthquake sequence consisted of a M6.4 rupture along the Salt Wells Valley left-lateral strike-slip fault on July 4th, 2019, followed by a M7.1 rupture of the nearly perpendicular Paxton Ranch right-lateral strike-slip fault on July 5th, 2019. Here we chose three sites, two along the Paxton Ranch fault and one along the Salt Wells Valley fault to investigate the paleoseismic rupture history of each of these faults. We excavated five trenches among the three sites. Each trench exposed evidence of past earthquake ruptures, although the timing remains uncertain pending dating results. The clearest event chronology was exposed in the trench at the basin site along the southern part of the Paxton Ranch fault, and showed clear evidence for at least two prior latest Pleistocene/Holocene surface rupturing events, with vertical displacements similar to the 2019 event. Assuming that the ~120 cm dextral displacement from the most recent event at this site was similar for each of these three total events and an estimate age of the oldest deposits based on the age of pluvial Searles Lake (~12 ka), we estimate a local slip rate of 0.3 mm/yr for the southernmost part of the fault. Due to the lower depositional rates at the other sites, unraveling a specific event chronology in the other trenches has proven challenging, however, future dating results will provide broad time constraints on prior deformation.

Introduction

The 2019 Ridgecrest earthquake sequence consists of two surface rupturing events: the July 4, 2019 M6.4 rupture of the northeast-striking left-lateral Salt Wells Valley fault and the nearly orthogonal July 5, 2019 M7.1 rupture of the northwest-striking right-lateral Paxton Ranch fault (Ponti et al., 2020). The Salt Wells Valley event produced ~18 km of surface rupture with a maximum left-lateral displacement of 0.7-1.6 m, while the Paxton Ranch event produced ~50 km of surface rupture with a maximum right-lateral displacement of 4.3-7.0 m (DuRoss et al., 2020).

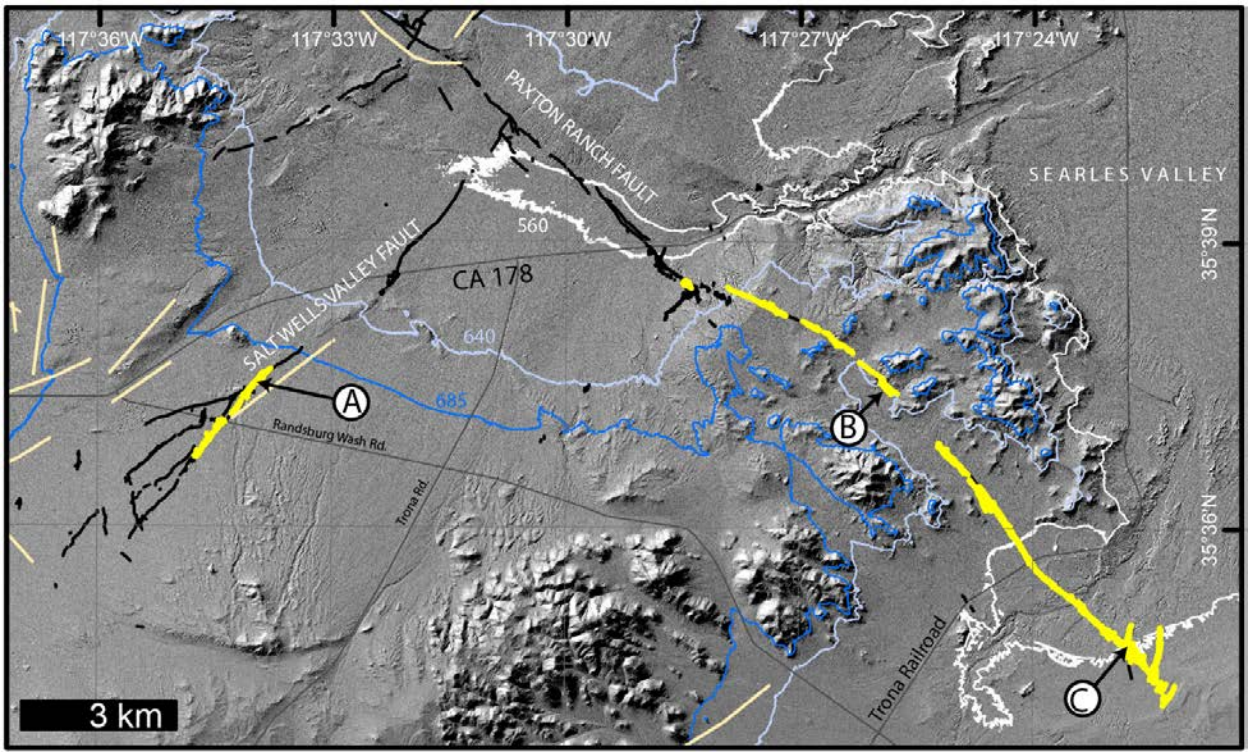

Figure 1. *Location map of southern part of 2019 Ridgecrest sequence. Yellow lines are 2019 surface ruptures mapped in previous related efforts by this group, black are ruptures of Ponti et al. 2019, and tan are faults from USGS Q-fault database. Light blue is ~12 ka 640 m highstand elevation, and darker blue is ~17 ka 685 m (Rosenthal et al., 2017). The Salt Wells Valley site is labeled as A, the Spangler Hills trench site is labeled as B, and the Basin trench as C.*

Background

The Ridgecrest earthquake sequence occurred in the Eastern California Shear Zone (ECSZ), which at the latitude of Ridgecrest apparently accommodates 10-12 mm/yr of northwest directed dextral shear (Dixon et al., 2000), or ~20% of the Pacific North-American Plate motion. The ECSZ is a locus of seismic activity, having experienced numerous large ruptures (e.g. Landers, Hector Mine, Owens Valley). The subsequent paleoseismic investigations of the faults that produced these earthquakes reveal evidence of prior earthquakes that occurred from ~5-15 ka (Beanland and Clark, 1994; Rubin and Sieh, 1997; Rockwell, 2000; Rymer et al., 2002). Like these other historic earthquakes in the ECSZ, the 2019 Ridgecrest earthquakes ruptured multiple faults, each with their own prior rupture histories.

In the days immediately following the two earthquakes, we collected >20,000 low-altitude UAV images to create high resolution (~2 cm/pixel) orthophotos with structure-from-motion (SfM) software along the publicly accessible (south of CA 178) portions of the 2019 M_w 6.4 and M_w 7.1 surface ruptures (Pierce et al., 2020). Our fault map based on these photos is shown in **Fig. 1** (yellow lines). A brief followup effort in September 2019 filled in holes in the datasets. The

initial results from this geodetic imaging show that the two surface ruptures produced fault zones of variable width, ranging from narrow zones dominated by a prominent fault to broad zones characterized by distributed surface cracks. Along much of both surface ruptures are features suggestive of prior earthquakes, including aligned ridges and drainages, small vertical scarps, and deflections of channels in young alluvial fans (Jobe et al., 2020). In this project, we excavated trenches across sites with geomorphic evidence of past rupture to constrain the timing of past earthquakes along each fault.

The pluvial Searles-China Lake history provides geomorphic context and limits the age of past ruptures. This lake level curve spans ~22,000-12,000 cal. yr BP, with lake levels from ~685-640 m (Fig. 4 of Rosenthal et al., 2017). Nearly all of the M_w 7.1 Paxton Ranch rupture is below the 640 m elevation, and thus most faulted geomorphic surfaces were formed less than ~12,000 cal. yr BP (light blue line in **Fig. 1**). Along the M_w 6.4 Salt Wells Valley rupture, part of the rupture is above the 685 m 17,000 cal. yr BP China Lake highstand (dark blue in **Fig. 1**), while other parts ruptured sediments below the elevation of the late Pleistocene highstand. As our post-earthquake reconnaissance found numerous locations with evidence of prior surface rupture in post-lacustrine alluvial fans below these elevations, we expect that the penultimate events that ruptured both faults will be early Holocene or latest Pleistocene in age, similar to the aforementioned ruptures in the ECSZ (Beanland and Clark, 1994; Rubin and Sieh, 1997; Rockwell et al., 2000; Rymer et al., 2002).

Methods

Trenches were cut personally using a rented excavator to lower the cost and provide freedom for exploratory digging. Exposures produced by the trenches across the faults were cleaned, photographed, and logged using established paleoseismic methods (e.g., McCalpin, 2009). Photographs were combined using Agisoft Metashape into orthomosaics of each trench wall. Units are divided based on color, composition (grain size, rounding, weathering, sorting, and stratification), interpretation of facies, and cross-cutting relations between stratigraphic deposits and faults. Faults are identified by the juxtaposition of units and zones of aligned shears. Upward terminating faults, juxtaposed units, cross-cutting relations, presence of fissures, and carbonate lined fractures are interpreted as evidence of past earthquakes.

Results

Salt Wells Valley fault

Along this section of the fault, there is a series of channels cutting through a low-relief fault aligned bedrock ridge. These channels were offset 90-150 cm left-laterally during the 2019 event. We selected a site where a young alluvial fan cut through uplifted granitic bedrock along the fault (**Figure 2**). Here we excavated two trenches. The Salt Wells Valley site is situated above the late Pleistocene highstand of Searles-China Lake at ~735 m elevation.

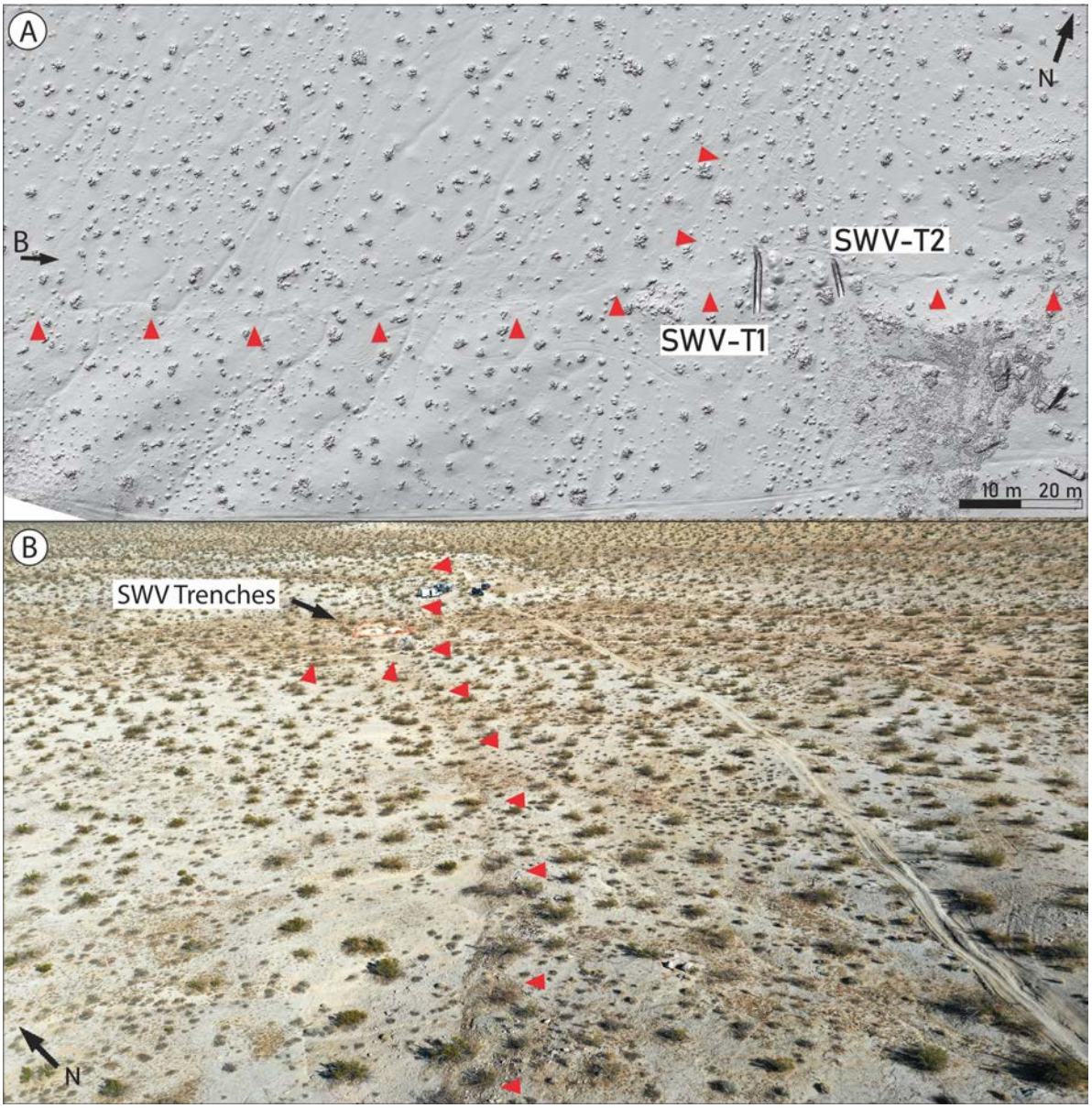

Figure 2. *Site map of the Salt Wells Valley fault showing trenches and offset channels. Fault trace is indicated with red arrows. Inset A displays hillshade derived from structure from motion model with Salt Wells Trench 1 (SWV-T1) and Trench 2 (SWV-T2). Black arrow indicates the orientation of the photo in inset B.*

SWV-T1

The T1 trench was situated on a pediment surface between a young active wash and an outcrop of granitic bedrock (**Figure 2**). The trench was excavated across a ~1.5 m right-step over in the surface rupture. The SWV-T1 trench (**Figure 3**) was primarily composed of fine grained gruss alluvium capping heavily sheared granite bedrock (unit 7) and indurated sediments (unit 6). Numerous carbonate lined fractures throughout the section do not reach the surface, and are buried by stratigraphic units, demonstrating past rupture of this fault (terminating below unit 2). OSL was sampled from units 1, 2, 3,4, and 6.

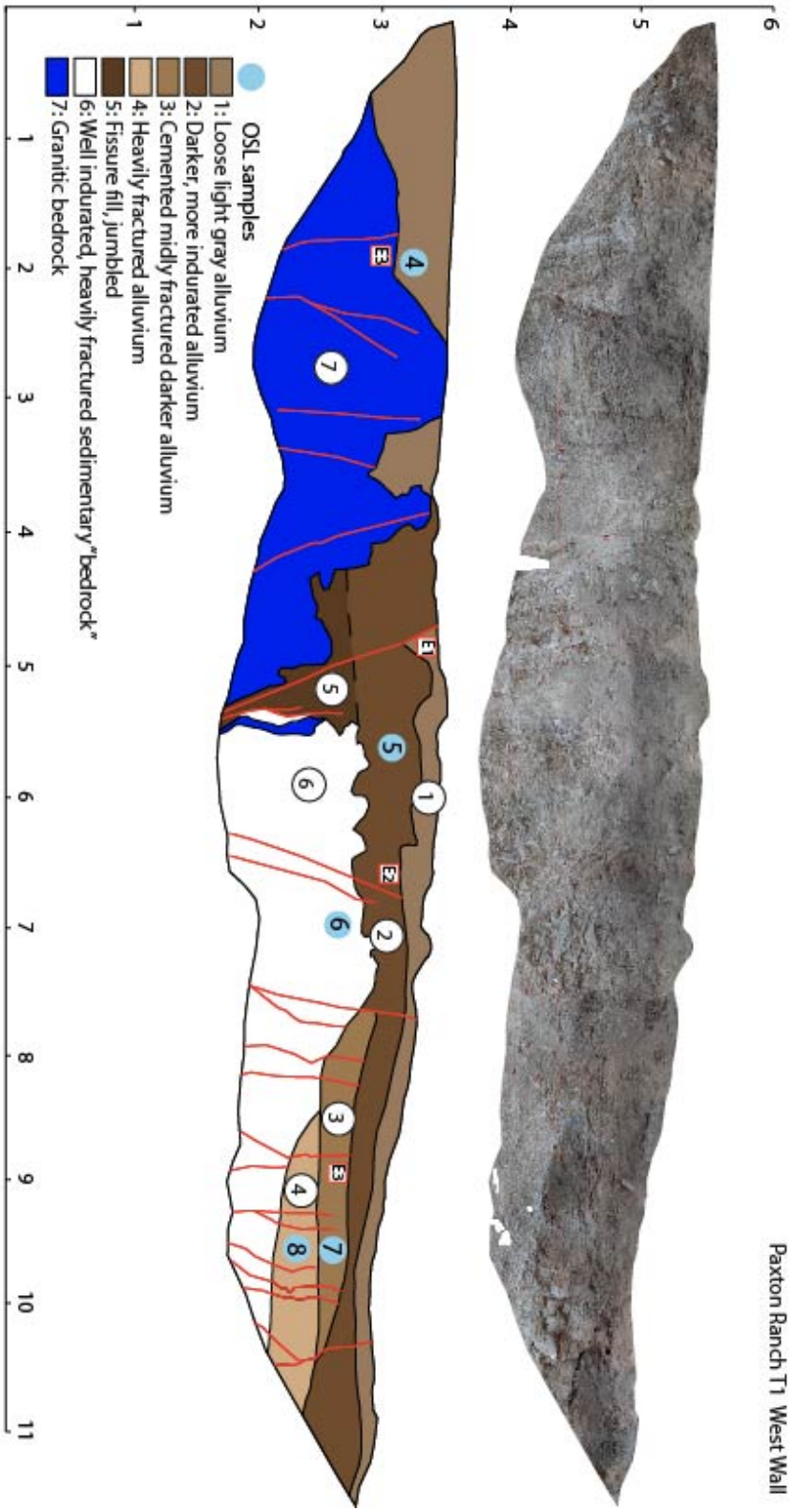

Figure 3 . *Trench Log for west wall of the SWV-T1 trench. Carbonate lined fractures throughout the trench exposure provide evidence of prior rupture along this fault.*

SWV-T2

The SWV-T2 trench (**Figure 4**) was situated across a small upstream-facing scarp in the center of a wash. The wash was composed of granitic gruss. Two fault traces reach the surface at this site. The exposure was primarily composed of granitic gruss with varying degrees of soil development (units 1-4), on top of an indurated sedimentary paleosurface (unit 5) exposed at the bottom of the trench. OSL was sampled in a vertical profile through units 2-4.

As vertical offsets are consistent across the section and all faults reach the surface we interpret this to only be a result of the 2019 event.

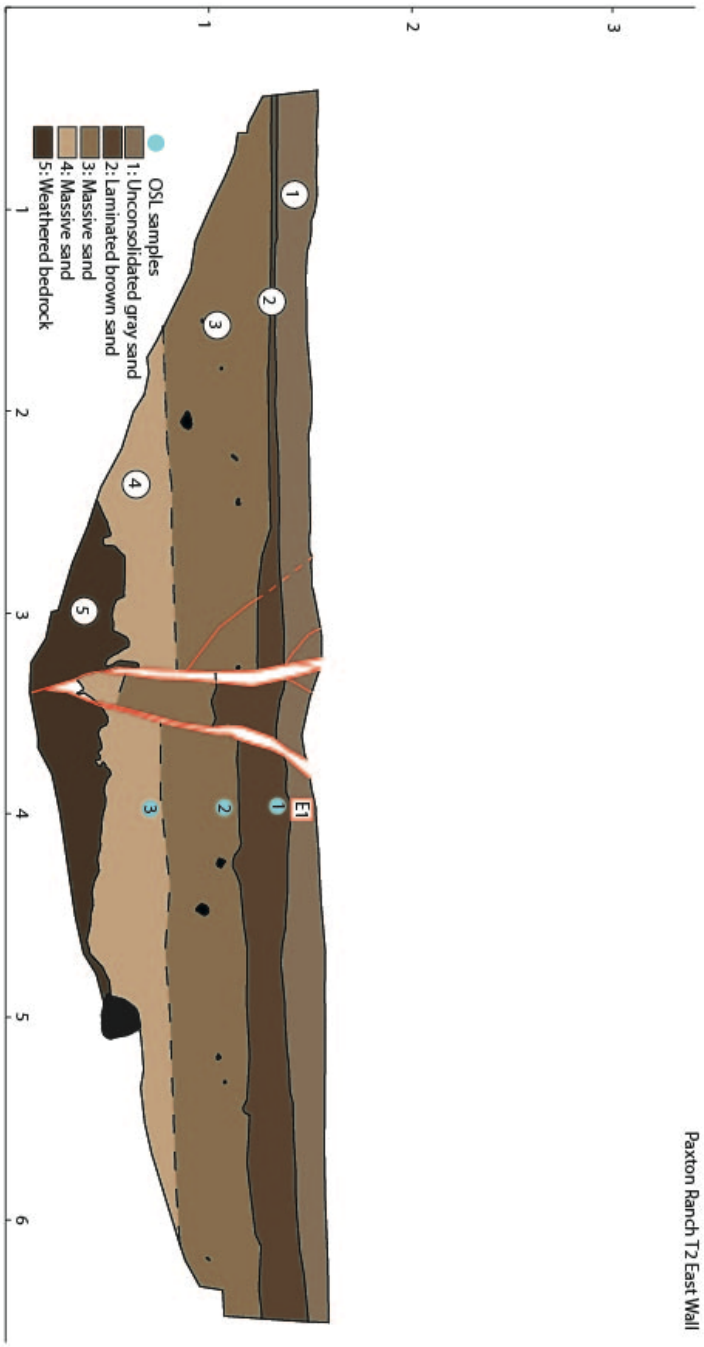

Figure 4 . *Trench log for the east wall of the SWV-T2 trench. Consistent offset along the entire section shows that the trench only preserves evidence of the 2019 event.*

Paxton Ranch fault

Two sites were selected for trenching along the southern part of the Paxton Ranch fault. The first site is near the crest of the Spangler Hills (SH), while the second site is in the central part of the Searles Lake basin.

Spangler Hills site

The Spangler Hills site is located near the crest of the Spangler Hills (**Figure 1**). It is situated at 650 m elevation, just below the 690 m highstand of Searles Lake (Rosenthal et al., 2017). There are two primary fault strands in this area, an eastern strand which runs along the small rangefront, and a western strand that cuts through alluvial deposits (**Figure 5**). The overall fault geometry here forms a right-stepover. Here two trenches were excavated across the western fault strand that cuts through a series of low relief fans and bedrock pediment surfaces. SH-T1 was excavated in an active channel, while SH-T2 was excavated in a young fan. Tufa deposits were present at the ground surface nearby on top of the young fan, suggesting this surface is approximately the age of the last highstand (~17.5 ka).

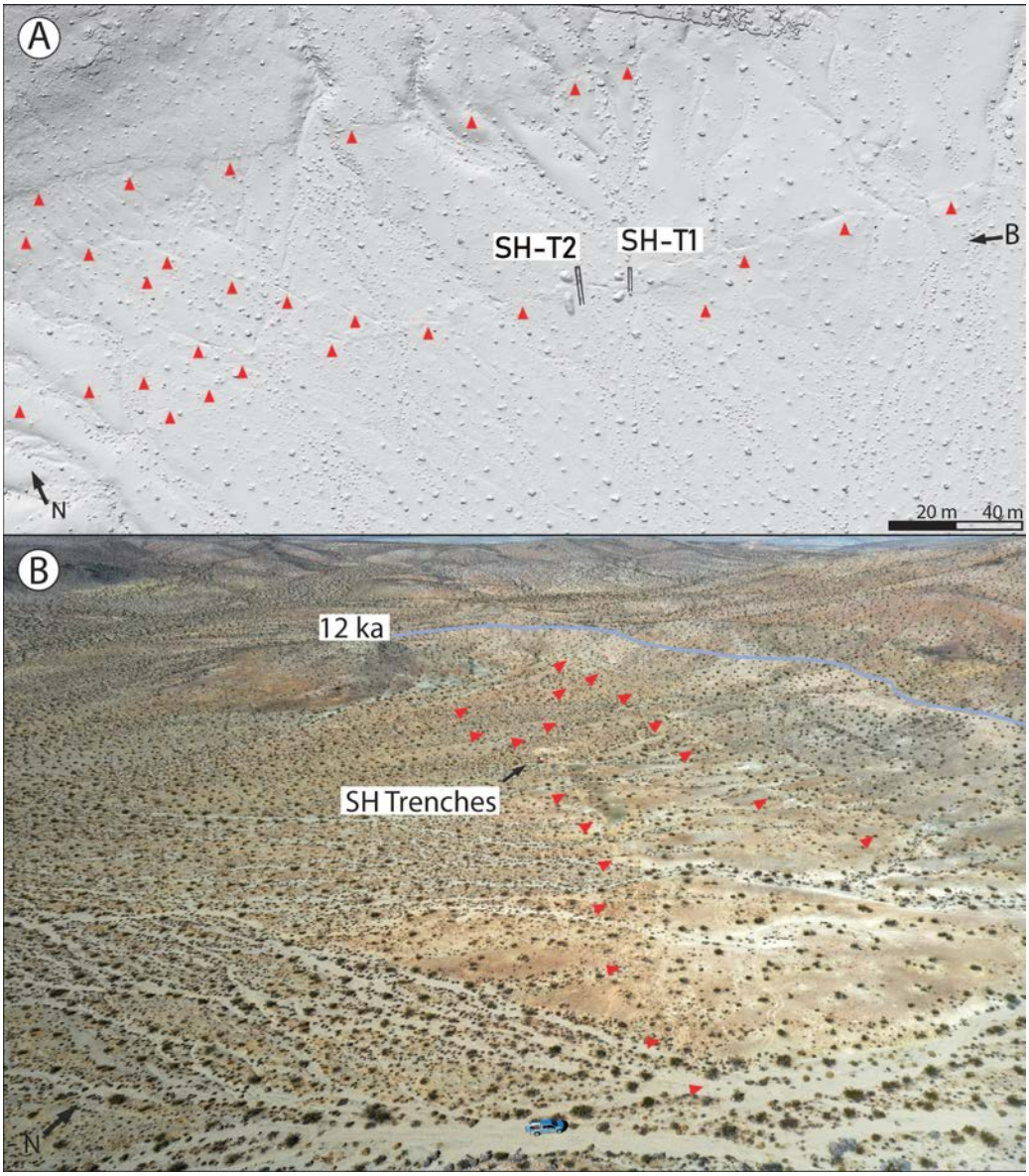

Figure 5. *Site map for Paxton Ranch fault showing Spangler Hills site. Fault trace is indicated with red arrows. Part A displays hillshade from Structure from Motion model of Spangler Hills*

Trench 1 (SH-T1) and Trench 2 (SH-T2). Black arrow indicates the orientation of oblique photo in inset B.

SH-T1

The SH-T1 trench (**Figure 6**) exposed a thin strath of weakly bedded, gravelly, loose gray/brown alluvial stratigraphy (unit 1) capping bedrock and lacustrine deposits. The fine grained silty/sandy lacustrine sediments are heavily indurated and can be broken into two subunits (units 2 and 3) based on color, texture, and an apparent contact within the unit. Small shells were recovered from shell-hash lenses within unit 3. The bedrock (unit 4) is locally heavily sheared and apparently overthrusts the lacustrine sediments. Two main fault traces broke the surface here in 2019. OSL was sampled from units 1, 2, and 3.

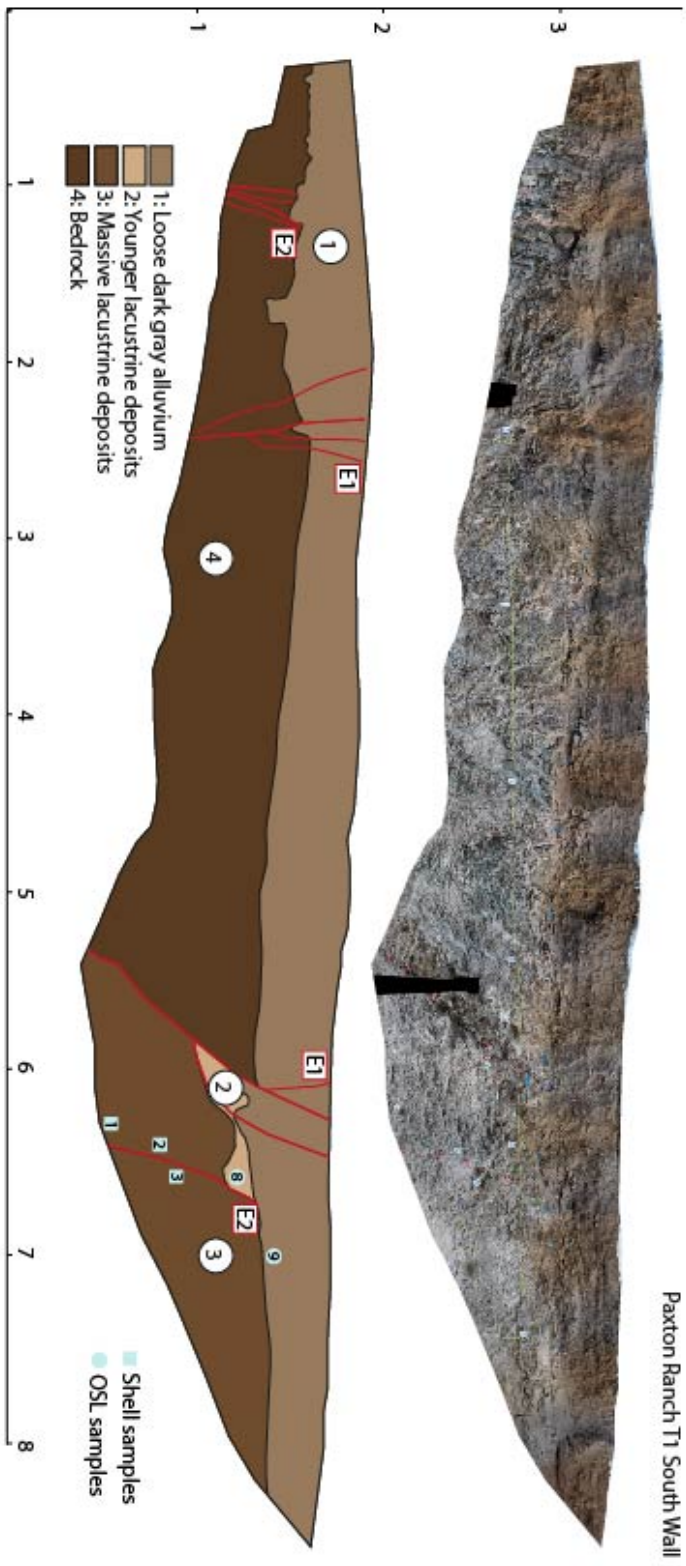

Figure 6. *SH-T1 trench log. Bedrock thrust over lacustrine sediments is likely the result of multiple events.*

SH-T2

The SH-T2 trench was excavated next to a mole track in the young fan across a section of en-echelon faults. The trench exposed a thin alluvial cap (unit 1), overlaying a sequence of faulted lacustrine beds (units 2-6). Units 2-4 are clearly bedded with a bleached paleosol surface at the top of unit 4. Units 5 and 6 are heavily indurated. The intervening shear zone (unit 7) consists of 5 primary en-echelon fault strands that each produced fissures during the 2019 event and overall form a weak positive flower structure. Many of these fissures reached a depth of at least 1.5 m, but it is unclear if they are a result of only the 2019 event or also an earlier event.. It is unclear how units 5 and 6 relate to units 2-4. Carbonate cemented cracks within units 3-6 provide evidence of rupture prior to the 2019 event. OSL was sampled from units 2,3, 4, 5, and 6.

Basin Site

The basin site is near the central part of the Searles Lake basin close to the southernmost part of the 2019 rupture (**Figure 1**). This site is at an elevation of ~580 m, well below the Searles lake highstand. Here, a wide wash is cut into lacustrine sediments and a small uphill (southwest) facing scarp was formed by the left-stepping fault running nearly perpendicular to the wash (**Figure 8**). The 2019 right-lateral displacements in this area are ~120 cm. The trench was excavated close to the northern margin of the wash. A thin (< 1 cm thick) silt/clay “playa” slackwater deposit formed behind the scarp since the 2019 event.

The trench exposed a very clear sequence of lacustrine and fluvial stratigraphy. The lacustrine sequence (units 3-8) consists of interbedded well sorted imbricated pebbles with massive fine sand and clay beds. Units 6-8 are fine sand beds, interpreted to be deeper water lacustrine deposits. Unit 5 is a coarse sand bed interpreted to be a beach deposit. Unit 4 is composed of well sorted fine pebbles and coarse sand that form clear backsets, suggesting an agrading beach sequence. Unit 3 is a clay package that either is a result of ponding behind a fault scarp (similar to observed on the ground surface following the 2019 rupture) or a deeper water lacustrine facies. These lacustrine units are interpreted to be a result of the most recent pluvial episode in Searles Lake (~12-17 ka, Rosenthal et al., 2017). The uppermost units 1 and 2 are laminated fluvial gravels and sands with localized clay lenses and cross-stratification, interpreted to be deposited by the modern wash following the lake’s recession and incision into the lacustrine sequence. The base of unit 2 is erosional into units 3 and 4.

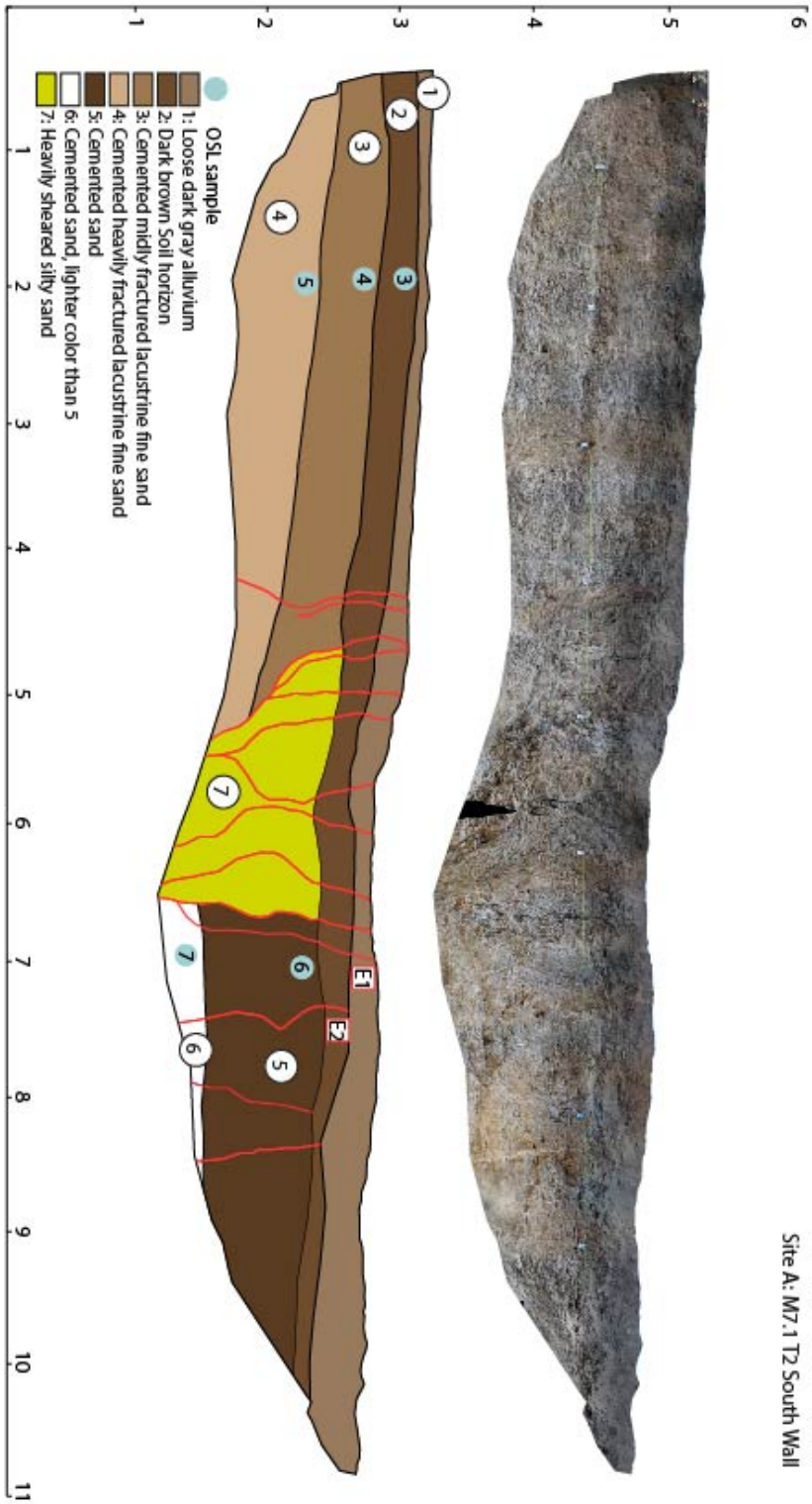

Figure 7. *SH-T2 log. A broad shear zone and carbonate cemented cracks in lacustrine sediments provide evidence of prior ruptures.*

The fault zone in this trench is well expressed with a reverse sense of motion. Based on upwardly terminating fault strands, we interpret evidence of two events prior to the 2019 surface rupture. The older event terminates within unit 4, while the younger event terminates at the top of unit 2. Each unit on the west side of the trench is much thicker than that on the east, consistent with repetition of local east-side uplift and infilling of the small local basin produced by this vertical motion. Furthermore, units 2-4 thin to the far west side of the trench, consistent with long term warping and infilling of the small basin produced by the fault.

Figure 8. *Oblique aerial photo of the M7.1 Basin trench site prior to excavation. Upstream facing scarp indicated by red arrows.*

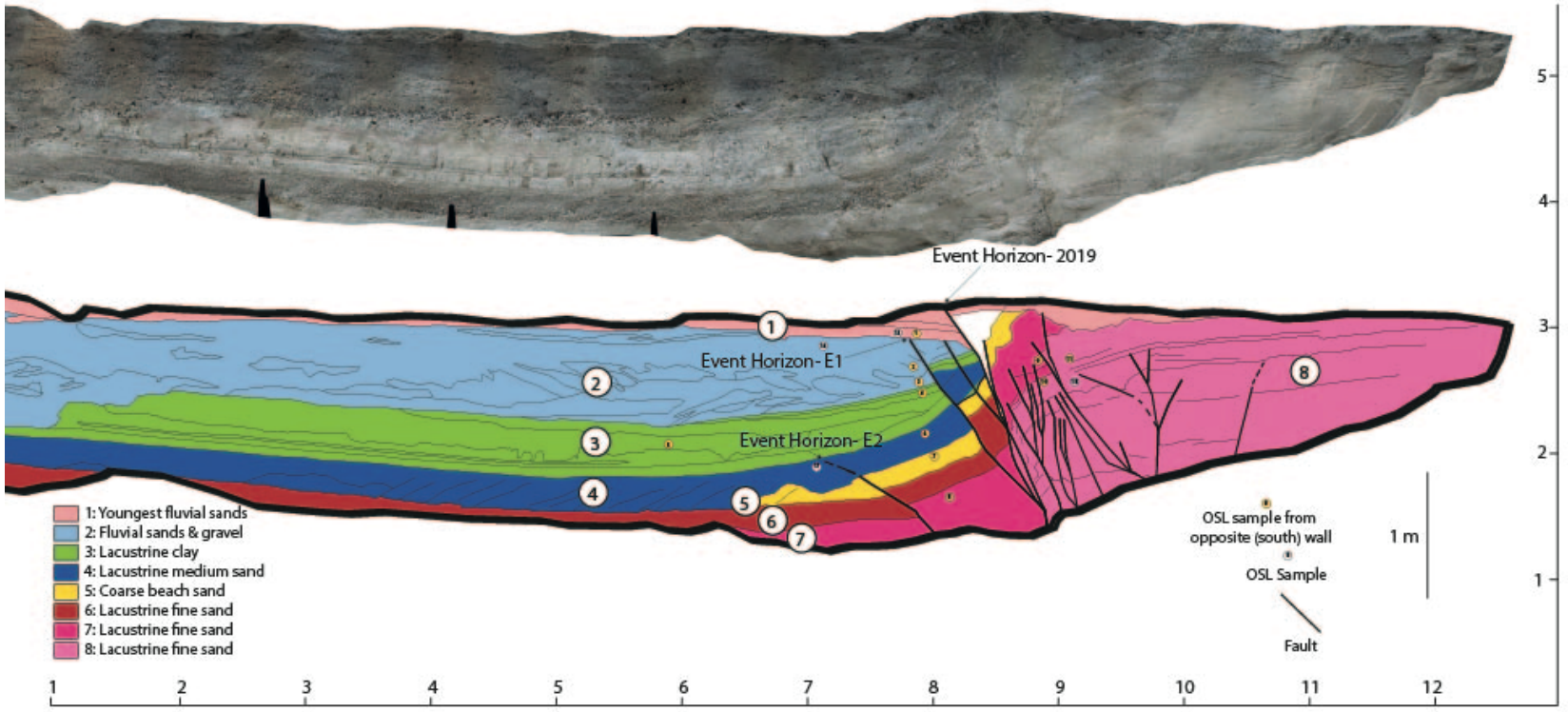
Event Horizon- 2019
Event Horizon- E1
Event Horizon- E2
1
2
3
4
5
6
7
8
1: Youngest fluvial sands
2: Fluvial sands & gravel
3: Lacustrine clay
4: Lacustrine medium sand
5: Coarse beach sand
6: Lacustrine fine sand
7: Lacustrine fine sand
8: Lacustrine fine sand
OSL sample from opposite (south) wall
OSL Sample
Fault
1 m
1
2
3
4
5
6
7
8
9
10
11
12

Figure 9. *(Prior page) Basin trench log. Fault terminations in units 2 and 4 provide evidence of 2-3 paleoearthquakes prior to the 2019 rupture. Units 3-8 are lacustrine deposits likely from the last lake cycle ~12-17 ka. OSL samples are indicated by yellow circles.*

Discussion

Evidence of past faulting

Both geomorphic and stratigraphic evidence of prior faulting is present at all three sites. The geomorphic evidence at each site consists primarily of aligned hills and subdued paleoscarps. Stratigraphic evidence of prior rupture consists of upwardly terminating fault strands, carbonate lined cracks, and shear zones exposed in the trenches.The basin trench on the Paxton Ranch fault provides clear evidence of at least two events prior to the 2019 rupture and since the late Pleistocene highstand of Searles Lake (~17 ka). The timing of past events on the Salt Wells Valley fault is unclear pending future dating results, but likely has produced several late Pleistocene events based on the amount of deformation observed in SWV-T1. Depositional rates at both the SWV and SH sites seemed to be very low, leading to thin Holocene deposits at the uppermost 10-20 cm of the trenches, and therefore obscuring conclusive evidence of multiple Holocene ruptures.

Slip Rate Estimates for the Paxton Ranch fault

The right-lateral displacement near the basin site along the Paxton Ranch fault in 2019 was ~120 cm. If the three events occurred since the last highstand of Searles Lake ~12 ka, and each event produced a similar displacement, then a latest Pleistocene slip rate of ~0.3 mm/yr can be inferred for the southern part of the fault. The max displacement observed during this event was ~5 m along the central part of the rupture (DuRoss et al., 2020). If this displacement was repeated for each of the 3 events over the same time frame, the maximum slip rate along the central part of the fault could be as high as ~1.3 mm/yr. Taken together these estimates range from 0.3-1.3 mm/yr. This rate is similar to other nearby faults in the Southern Walker Lane and is in line with geodetic estimates across the region (e.g., Pierce et al., 2021).

Variation in character of surface rupture observed from trenches

The trench sites show considerable variation in the expression of near surface fault rupture. The character of rupture varied immensely at both the SWV and SH sites, even over the short ~20 m distances between the adjacent trenches. Fissures were observed in most of the trenches, reaching depths as great as ~2 m, but with widths generally <10 cm. It is unclear if these fissures are the result of solely the 2019 event or are overprinted over earlier events. While we tried to target relatively simple surficial fault expressions, deformation widths observed in the trenches varied from relatively narrow along a simple fault geometry (~1 m wide for SWV-T2 or SH-T1), to ~10 m wide along more complex sections (SWV-T1). We did not trench any of the wider rupture zones observed on the surface, which were as wide as ~100 m in some cases. Trench SH-T1 contained multiple fault strands, each with a narrow deformation zone, separated by a wide zone of undeformed strata, while both SWV-T1 and SH-T2 contained a broad zone of

nearly continuous deformation. SWV-T1 showed a complex stepover zone. Trench SWV-T2 revealed an extensional component of faulting with a downdropped graben. SH-T1 and the basin trench both revealed faulting with a significant reverse component, but with opposite relative motions (east side down vs. east side up). SH-T2 revealed a positive flower structure, with limited vertical motion across the numerous echelon fault strands.

References

Beanland, S., Clark, M.M., 1994. The Owens Valley Fault Zone, Eastern California, and Surface Faulting Associated with the 1872 Earthquake (U.S. Geological Survey Bulletin No. 1982). U.S. Geological Survey.

Dixon, T.H., Miller, M., Farina, F., Wang, H., Johnson, D., 2000. Present-day motion of the Sierra Nevada block and some tectonic implications for the Basin and Range province, North American Cordillera. Tectonics 19, 1–24.

DuRoss, C.B., Gold, R.D., Dawson, T.E., Scharer, K.M., Kendrick, K.J., Akciz, S.O., Angster, S.J., Bachhuber, J., Bacon, S., Bennett, S.E.K., Blair, L., Brooks, B.A., Bullard, T., Burgess, W.P., Chupik, C., DeFrisco, M., Delano, J., Dolan, J.F., Frost, E., Graehl, N., Haddon, E.K., Hatem, A.E., Hernandez, J.L., Hitchcock, C., Hudnut, K., Thompson Jobe, J., Koehler, R., Kozaci, O., Ladinsky, T., Madugo, C., McPhillips, D.S., Milliner, C., Morelan, A., Olson, B., Patton, J., Philibosian, B., Pickering, A.J., Pierce, I., Ponti, D.J., Seitz, G., Spangler, E., Swanson, B., Thomas, K., Treiman, J., Valencia, F., Williams, A., Zinke, R., 2020. Surface Displacement Distributions for the July 2019 Ridgecrest, California, Earthquake Ruptures. Bull. Seismol. Soc. Am. 110, 1400–1418. https://doi.org/10.1785/0120200058

Jobe, J.A.T., Philibosian, B., Chupik, C., Dawson, T., Bennett, S.E.K., Gold, R., DuRoss, C., Ladinsky, T., Kendrick, K., Haddon, E., Pierce, I., Swanson, B., Seitz, G., 2020. Evidence of Previous Faulting along the 2019 Ridgecrest, California, Earthquake Ruptures. Bull. Seismol. Soc. Am. https://doi.org/10.1785/0120200041

McCalpin, J., 2009. Paleoseismology, 2nd ed. Academic Press.

Pierce, I., Williams, A., Koehler, R.D., Chupik, C., 2020. High-Resolution Structure-From-Motion Models and Orthophotos of the Southern Sections of the 2019 Mw 7.1 and 6.4 Ridgecrest Earthquakes Surface Ruptures. Seismol. Res. Lett. 91, 2124–2126. https://doi.org/10.1785/0220190289

Pierce, I.K.D., Wesnousky, S.G., Owen, L.A., Bormann, J.M., Li, X., Caffee, M., 2021. Accommodation of Plate Motion in an Incipient Strike-Slip System: The Central Walker Lane. Tectonics 40, e2019TC005612. https://doi.org/10.1029/2019TC005612

Ponti, D.J., Blair, J.L., Rosa, C.M., Thomas, K., Pickering, A.J., Akciz, S., Angster, S., Avouac, J., Bachhuber, J., Bacon, S., Barth, N., Bennett, S., Blake, K., Bork, S., Brooks, B., Bullard, T., Burgess, P., Chupik, C., Dawson, T., DeFrisco, M., Delano, J., DeLong, S., Dolan, J., Donnellan, A., DuRoss, C., Ericksen, T., Frost, E., Funning, G., Gold, R., Graehl, N., Gutierrez, C., Haddon, E., Hatem, A., Helms, J., Hernandez, J., Hitchcock, C., Holland, P., Hudnut, K., Kendrick, K., Koehler, R., Kozaci, O., Ladinsky, T., Leeper, R., Madugo, C., Mareschal, M., McDonald, J., McPhillips, D., Milliner, C., Mongovin, D., Morelan, A., Nale, S., Nevitt, J., O'Neal, M., Olson, B., Oskin, M., Padilla, S., Patton, J., Philibosian, B., Pierce, I., Pridmore, C., Roth, N., Sandwell, D., Scharer, K., Seitz, G., Singleton, D., Smith-Konter, B., Spangler, E., Swanson, B., Jobe, J.T., Treiman, J., Valencia, F., Vanderwal, J., Williams, A., Xu, X., Zachariasen, J., Zimmerman, J., Zinke, R., 2020. Documentation of Surface Fault Rupture and Ground-Deformation Features Produced by the 4 and 5 July 2019 Mw 6.4 and Mw 7.1 Ridgecrest Earthquake

Sequence. Seismol. Res. Lett. 91, 2942–2959. https://doi.org/10.1785/0220190322
Rockwell, T.K., 2000. Paleoseismology of the Johnson Valley, Kickapoo, and Homestead Valley Faults: Clustering of Earthquakes in the Eastern California Shear Zone. Bull. Seismol. Soc. Am. 90, 1200–1236. https://doi.org/10.1785/0119990023
Rosenthal, J.S., Meyer, J., Palacios-Fest, M.R., Young, D.C., Ugan, A., Byrd, B.F., Gobalet, K., Giacomo, J., 2017. Paleohydrology of China Lake basin and the context of early human occupation in the northwestern Mojave Desert, USA. Quat. Sci. Rev. 167, 112–139. https://doi.org/10.1016/j.quascirev.2017.04.023
Rubin, C.M., Sieh, K., 1997. Long dormancy, low slip rate, and similar slip-per-event for the Emerson fault, eastern California shear zone. J. Geophys. Res. Solid Earth 102, 15319–15333. https://doi.org/10.1029/97JB00265
Rymer, M.J., Seitz, G.G., Weaver, K.D., Orgil, A., Faneros, G., Hamilton, J.C., Goetz, C., 2002. Geologic and Paleoseismic Study of the Lavic Lake Fault at Lavic Lake Playa, Mojave Desert, Southern California. Bull. Seismol. Soc. Am. 92, 1577–1591. https://doi.org/10.1785/0120000936